# Proton Conduction in Tetra-*n*-butylammonium Bromide Semiclathrate Hydrate

Jin Shimada[1,2,3,4], Yuta Takaoka[5], Takahiro Ueda[6,7], Atsushi Tani[3], Takeshi Sugahara[1,2,*], Katsuhiko Tsunashima[8,*] Hirohisa Yamada[9], Takayuki Hirai[1,2]

[1]Division of Chemical Engineering, Department of Materials Engineering Science, Graduate School of Engineering Science, Osaka University, 1-3 Machikaneyama, Toyonaka, Osaka 560-8531, Japan

[2]Division of Energy and Photochemical Engineering, Research Center for Solar Energy Chemistry, Graduate School of Engineering Science, Osaka University, 1-3 Machikaneyama, Toyonaka, Osaka 560-8531, Japan

[3]Department of Human Environmental Science, Graduate School of Human Development and Environment, Kobe University, 3-11 Tsurukabuto, Nada, Kobe, Hyogo 657-8501, Japan

[4]Research Fellow of Japan Society for the Promotion of Science, 5-3-1 Kojimachi, Chiyoda-ku, Tokyo 102-0083, Japan

[5]Department of Material Science, National Institute of Technology, Wakayama College, 77 Noshima, Nada, Gobo, Wakayama 644-0023, Japan

[6]Department of Chemistry, Graduate School of Science, Osaka University, 1-13 Machikaneyama, Toyonaka, Osaka 560-0043, Japan

[7]The Museum of Osaka University, Osaka University, 1-13 Machikaneyama, Toyonaka, Osaka 560-0043, Japan

[8]Department of Applied Chemistry and Biochemistry, National Institute of Technology, Wakayama College, 77 Noshima, Nada, Gobo, Wakayama 644-0023, Japan

[9]Department of Chemical Engineering, National Institute of Technology, Nara College, 22 Yata, Yamatokoriyama, Nara 639-1080, Japan

**KEYWORDS.** Semiclathrate hydrate, Proton conduction, Isotope effect, Water reorientation, Electrochemical impedance spectroscopy

## ABSTRACT

Clathrate hydrate as well as ice has been spotlighted as promising materials to investigate the properties of hydrogen-bonded networks formed by the water molecules. In the semiclathrate hydrate (SCH, a kind of clathrate hydrate) consisting of host water molecules and guest quaternary onium salts, the anion takes part in the hydrogen-bonded networks with the water molecules. In the present study, we measured the electrical conductivity and electrical relaxation time in the single-crystalline tetra-*n*-butylammonium bromide (TBAB) SCH by electrochemical impedance spectroscopy. The results clearly revealed that the conduction carrier was proton. The electrical relaxation time of proton conduction in TBAB SCH was similar to the reorientation time of the water molecules in TBAB SCH estimated by the results of nuclear magnetic resonance.

## 1. INTRODUCTION

Both ice and clathrate hydrates, the important components on the planets, are crystalline compounds that consist of hydrogen-bonded networks of the water molecules.[1-4] Many researchers have been fascinated by their interesting properties. Among them, the electrical conductivity in hexagonal ice (hereafter ice Ih) is 10–100 times higher than that in liquid water.[5,6] The conduction mechanism in ice Ih has been proposed by Jaccard[7-9] and Onsager and Dupuis[10]. According to their proposed mechanism, charge conducts through a combination of ionic defect transfer and Bjerrum defect transfer. Ionic defect, such as $H_3O^+$ and $OH^-$ ions, is formed by proton-jump, the interaction between water molecules and neighboring polarized compounds, and thermal fluctuation. The Bjerrum defect[11] consists of a bond occupied by two protons (D defect) and of an empty bond (L defect)[12] between two oxygen atoms of water molecules. The mechanism of proton conduction in ice Ih has been reported as follows [13]: 1) ionic defects ($H_3O^+$ and $OH^-$) are formed; 2) the formed protons migrate along with the hydrogen-bonded water networks; 3) at Bjerrum defects, proton transfer is suspended because the proton cannot jump to neighboring water molecules; 4) after rearrangement of water molecules around Bjerrum defects, protons restart to jump. The water reorientation motion at Bjerrum defects plays a significant role in determining the apparent diffusion coefficient of protons. In other words, the reorientation of water molecules is the rate-limiting step of proton conduction mechanism in ice Ih system.[13]

In the case of clathrate hydrates, especially polycrystalline $CH_4$ hydrate and $CO_2$ hydrate, it has been reported that their electrical conductivities are similar to that in ice Ih,[14] whereas the relation between the diffusion and reorientation rates of water molecules in clathrate hydrate is different from that in ice Ih.[2] Concretely speaking, in ice Ih, the diffusion jump of water

molecules is about 8 times faster than the reorientation of water molecule, whereas, in clathrate hydrates, the diffusion jump is 20 times slower than the reorientation. In specific, the diffusion of water molecules in clathrate hydrate is two-order slower than that of ice Ih. The reorientation of water molecules in clathrate hydrate is twice faster than that in ice.

Interestingly, a clathrate hydrate containing ionic guest substance, called "semiclathrate hydrate (or ionic clathrate hydrate)", shows an electrical conductivity higher than clathrate hydrates and ice Ih. Semiclathrate hydrate is a kind of clathrate hydrates and consists of host water molecules and guest quaternary ammonium or phosphonium salts.[15-17] Four butyl groups on the cations are incorporated in the conjunct hydrate cage, where a part of the water molecules in the hydrate frameworks are replaced with the anion, that is, anion species behave as a part of the host substances.[18-20] The characteristics of semiclathrate hydrate are somewhat different from those of clathrate hydrate. One of them is that semiclathrate hydrate is stable under a relatively high-temperature condition even at atmospheric pressure. Opallo et al. systematically reported the electrochemical conductivity of polycrystalline semiclathrate hydrates formed from the several guest ions.[21-28] However, the carrier ion and/or conduction mechanism in semiclathrate hydrates have been not yet clear.

In the present study, to elucidate the carrier ion and to discuss the conduction mechanism in semiclathrate hydrates, electrochemical impedance spectroscopy (EIS) measurement was conducted. As a measurement sample, single-crystalline tetra-*n*-butylammonium bromide (TBAB) semiclathrate hydrate was used, because EIS is sensitive to the existence of grain boundary and metastable phases.[29] In addition, TBAB is one of the famous semiclathrate hydrate formers.[15,16,18,20,30] In TBAB semiclathrate hydrate ($TBAB \cdot 26H_2O$), the equilibrium temperature is 284.8–285.2 K [31-34] and the crystal structure is tetragonal (space

group: P4/*mmm*, lattice parameter: $a$ = 2.39(2) nm, $c$ = 5.08(5) nm).[35] In the TBAB semiclathrate hydrate, the existence of some metastable phases has been reported, which have different physicochemical properties (*e.g.* TBAB·38$H_2O$, TBAB·32.6$H_2O$, TBAB·32$H_2O$, and TBAB·24$H_2O$).[31] The single-crystalline semiclathrate hydrate was prepared to avoid the effects of metastable structures and grain boundaries in the EIS measurement. Furthermore, to discuss the conduction mechanism in semiclathrate hydrate, we measured $^2H$ nuclear magnetic resonance (NMR) of heavy water molecules in TBAB semiclathrate deuterate.

## 2. EXPERIMENTAL

### Samples

The TBAB reagent with minimum purity of 99.9 wt% was obtained from FUJIFILM Wako Pure Chemical Corporation. Distilled and deionized water was prepared in our laboratory (resistivity: 17.9 MΩ·cm). For the preparation of a single-crystalline TBAB semiclathrate hydrate, TBAB aqueous solution with the TBAB mass fraction ($w_{TBAB}$) of 0.400 was prepared, which is very close to the stoichiometric composition of TBAB·26$H_2O$. To confirm the isotope effect between $H_2O$ and $D_2O$, the experiment with $D_2O$ instead of $H_2O$ was also conducted in the same way, where $w_{TBAB}$ was 0.407. $D_2O$ with minimum purity of 99.9 atomic% was obtained from Cambridge Isotope Laboratories, Inc.

### Apparatus and procedure

The schematic illustration of experimental apparatus of EIS is shown in Figure 1. Approximately 1 $cm^3$ of TBAB aqueous solution was poured in an electrochemical measurement cell, which was fabricated from a pair of Pt disk electrodes (electrode area: 0.283 $cm^2$, distance between electrodes: 1.0 mm) with glass T-tube (VIDTEC). The cell was immersed in the ethylene glycol solution, where the temperature was kept at 285.1 K. The seed crystal of TBAB semiclathrate hydrate was added into the aqueous solution to prepare the single crystal. After a transparent crystal without grain boundaries was prepared in the space between electrodes (Figure 2), the temperature was gradually decreased at a rate of 0.1 K/1.5 hours and kept constant at least 1 hour prior to impedance measurement.

Figure 3 shows the impedance spectra of the single-crystalline and polycrystalline semiclathrate hydrates formed at 285 K (in panel A) and the spectra of semiclathrate hydrates formed at different temperatures (in panel B), where *Z*' and *Z*'' represent real and imaginary parts of impedance, respectively. The impedance in the polycrystalline TBAB semiclathrate hydrate depended largely on the formation temperatures of the polycrystalline samples. Thus, polycrystalline semiclathrate hydrates, without any treatments, should not be suitable for evaluation of ion conduction properties using EIS because of the effects of grain boundaries,[29] quasi-liquid layer,[36,37] and metastable phases.[21,38] In the present study, to eliminate the effect of grain boundaries and metastable phases in the EIS measurement, we prepared a single-crystalline TBAB semiclathrate hydrate in the space between both electrodes. Note that the existence of other crystals outside an effective region between both electrodes has no effect on the EIS. In lowering temperatures, gradual temperature change was needed to avoid the appearance of cracks in the single crystal.

The electrochemical impedance of semiclathrate hydrate was investigated by an impedance analyzer (SP-150, Bio-Logic Sciences Instruments Ltd) in a frequency range from 1 Hz to 100 kHz at atmospheric pressure. The 500 mV of sinusoidal signal (peak-to-peak amplitude) was applied to the cell. The impedance results were calibrated with the cell constant obtained in 0.01 M KCl aqueous solution.

The impedance data have been analyzed with a following equivalent circuit (1):[22,23]

$$Z = R_{\mathrm{sol}} + \frac{R_{\mathrm{hyd}}}{1 + (j\omega)^{p_{\mathrm{hyd}}} R_{\mathrm{hyd}} Q_{\mathrm{hyd}}} + \frac{1}{(j\omega)^{p_{\mathrm{dl}}} Q_{\mathrm{dl}}} \quad (1)$$

where, $Z$, $R$, $j$, ω, $p$, and $Q$ are impedance, resistance, imaginary unit, angular frequency, fractional exponent of constant phase element, and coefficient of constant phase element, respectively. The subscripts sol, hyd, and dl correspond to aqueous solution, semiclathrate hydrate, and electric double-layer, respectively. In the present study, resistance in aqueous solution was negligible because the resistance was infinitesimally small. Therefore, the impedance results were analyzed with an equivalent circuit (2).

$$Z = \frac{R_{\mathrm{hyd}}}{1 + (j\omega)^{p_{\mathrm{hyd}}} R_{\mathrm{hyd}} Q_{\mathrm{hyd}}} + \frac{1}{(j\omega)^{p_{\mathrm{dl}}} Q_{\mathrm{dl}}} \tag{2}$$

Capacitance ($C$) was estimated from following equation (3):

$$C_{\mathrm{hyd}} = Q_{\mathrm{hyd}}{}^{\frac{1}{p_{\mathrm{hyd}}}} (R_{\mathrm{hyd}})^{\frac{1-p_{\mathrm{hyd}}}{p_{\mathrm{hyd}}}} \tag{3}$$

The electrical conductivity (σ) and relaxation time (τ) obtained by EIS were calculated from the resistance ($R$) and capacitance ($C$), as the following equations (4) and (5):

$$\sigma = \frac{1}{R_{\mathrm{hyd}}} \frac{d}{A} \tag{4}$$

$$\tau = 2\pi R_{\mathrm{hyd}} C_{\mathrm{hyd}} \tag{5}$$

where the symbols $d$ and $A$ represent the distance between two Pt electrodes and the electrode area, respectively.

Solid-state $^2$H NMR was conducted using AVANCE 600 (Bruker) equipped by a superconducting magnet with the magnetic field of 14.1 T, which corresponds to the resonance frequency of 92.129 MHz for $^2$H nuclei. TBAB semiclathrate deuterate was formed around 250

K and annealed at 284.2 K for 3 days in an NMR sample tube to avoid the coexistence of metastable phases. The $T_1$ and $T_2$ relaxation times were measured using inversion recovery [180° – $t$ – 90°] and solid echo [90° – $t$ – 90°] methods, respectively. The pulse length of 90° and 180° pulses were 6.25 μs and 12.5 μs, respectively. The line width of the narrow peaks reflects the temperature-independent ($\nu^0_{1/2}$) and the temperature-dependent [$\nu_{1/2}(T)$] components. The former is the intrinsic line width, and the latter corresponds to the motional narrowing part which is proportional to the spin-spin relaxation rate ($1/T_2$) in the extreme narrowing region.[39,40] In order to examine the isotropic reorientation motion of water molecules, we estimated the activation energy using narrow peak width.

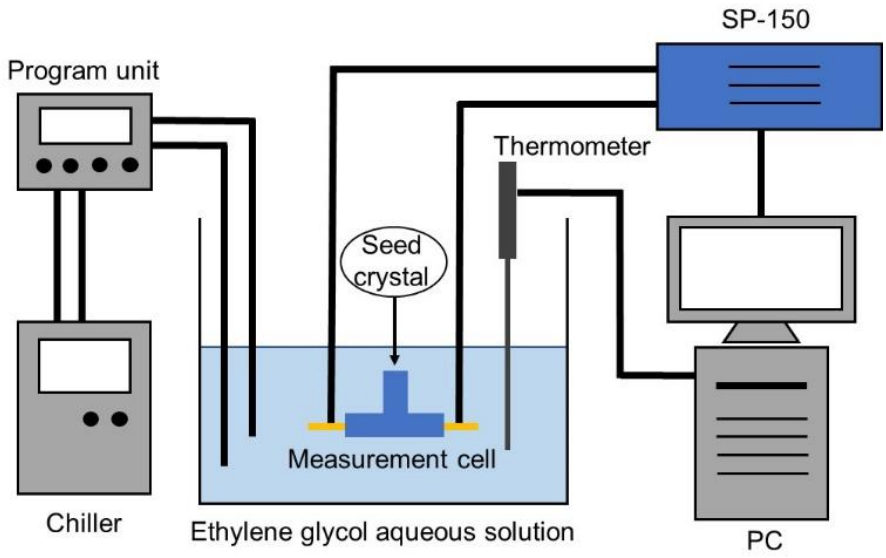


Figure 1. Schematic illustration of the apparatus for the electrochemical impedance measurement.

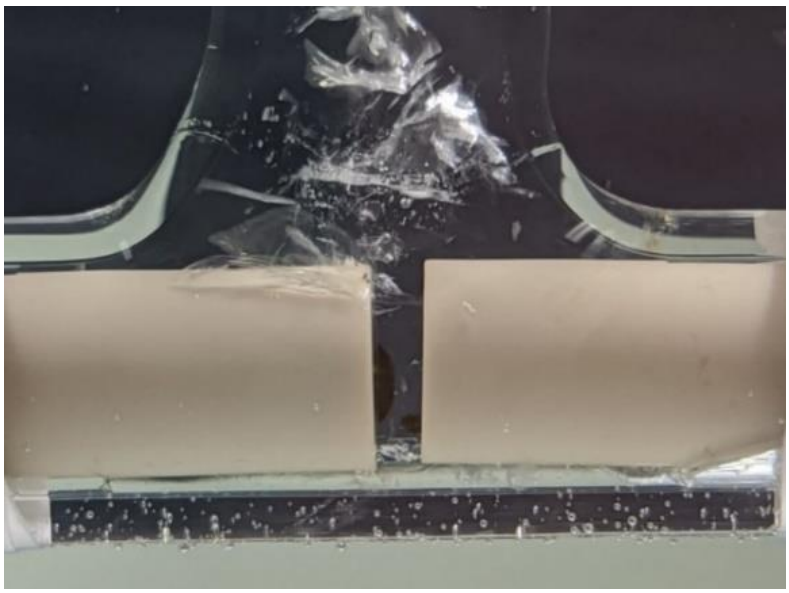

Figure 2. Typical photo of single-crystalline TBAB semiclathrate hydrate formed between Pt electrodes. The surfaces of both electrodes were completely covered with a single crystal, though grain boundaries were present outside the effective region between electrodes.

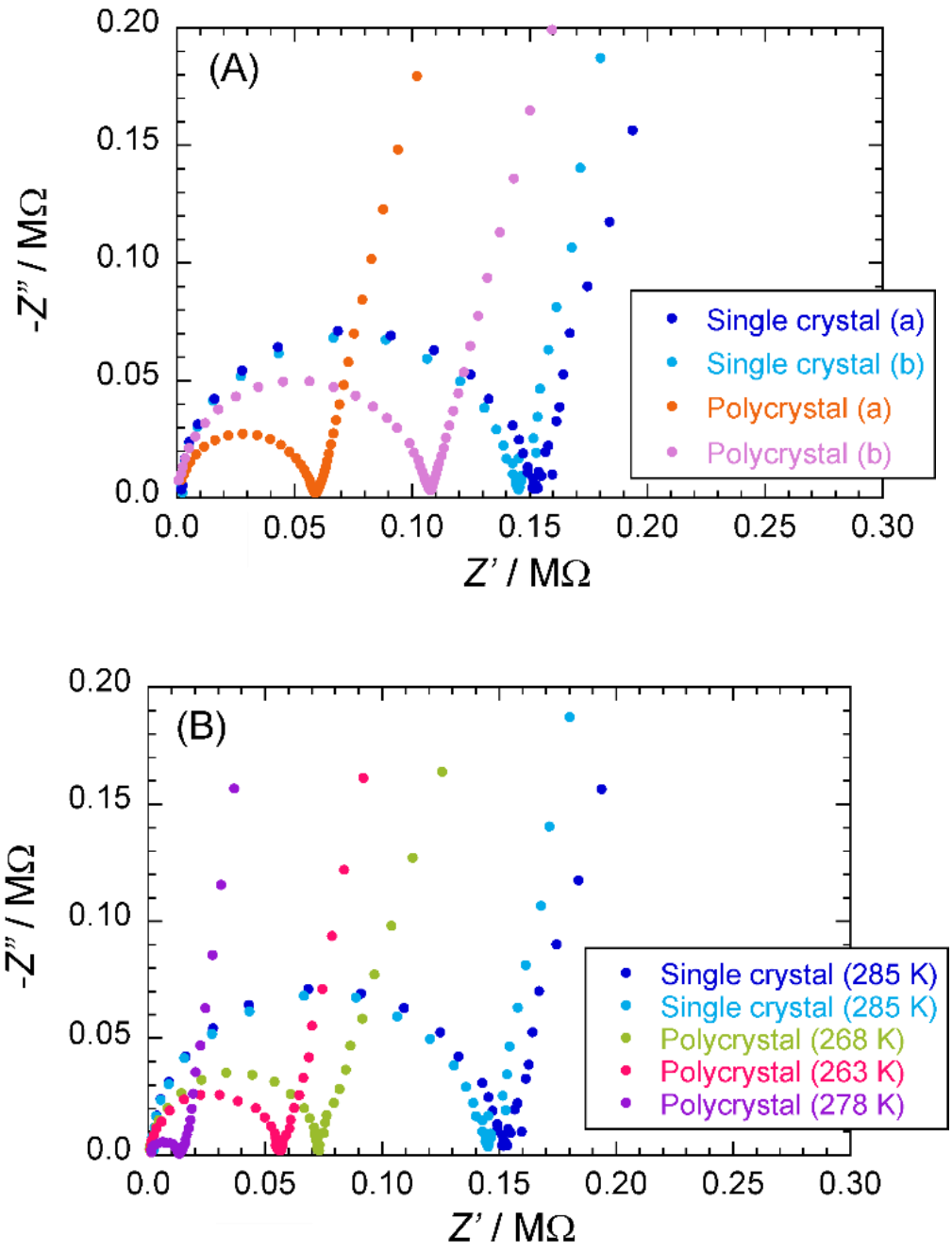


Figure 3. (A) Typical Nyquist plots of single crystals and polycrystals formed at 285 K. All spectra were measured at 283 K. Notations of (a) and (b) in single crystals and polycrystals indicate different crystals prepared with the same procedure. (B) Typical Nyquist plots of single crystals formed at 285 K and polycrystals formed at 263, 268, and 278 K. All spectra were measured at 283 K.

## 3. RESULTS AND DISCUSSION

### Temperature dependence of impedance in TBAB semiclathrate hydrates

Figures 4 and 5 show temperature dependences on Bode plots and Nyquist plots in a single-crystalline TBAB semiclathrate hydrate, respectively. In Figure 5, a high-frequency arc and a low-frequency tail were observed. Since the TBAB semiclathrate hydrate used in the present study was a single crystal without grain boundaries between the electrodes, there was neither impedance derived from a metastable phase nor grain boundaries. Therefore, the bulk resistance of semiclathrate hydrate $R_{hyd}$ was determined from the intersection of the low frequency tail with the real axis of the impedance $Z$'. The resistance in TBAB semiclathrate hydrate was increased with a decrease in measurement temperature. Such behavior has been frequently seen in the typical ionic conductors.[41,42]

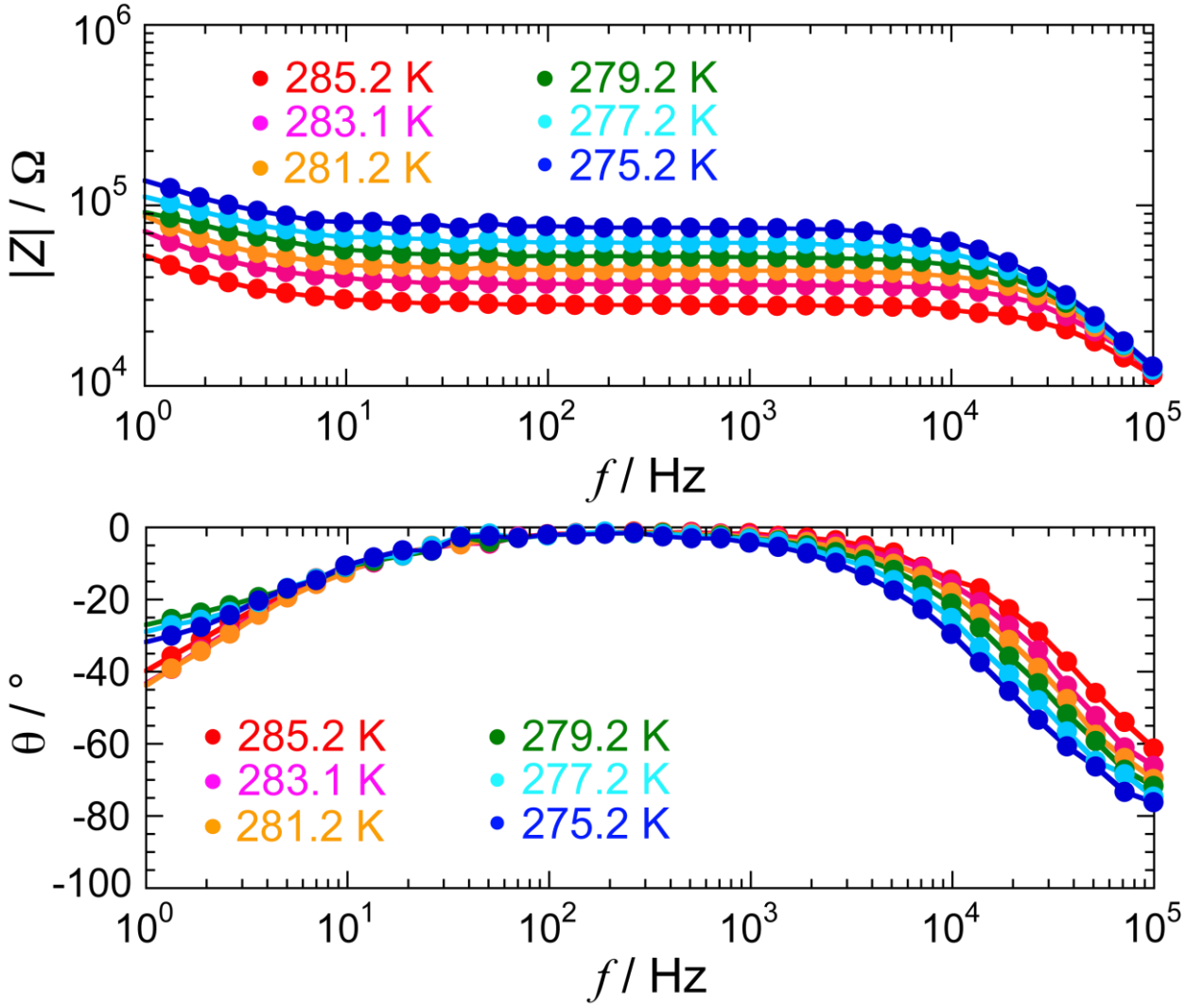


Figure 4. Bode plots of EIS measured at various temperatures in the single-crystalline TBAB semiclathrate hydrate (electrode area: 0.283 $cm^2$, distance between electrodes: 1.0 mm). $|Z|$ and θ stand for impedance and phase delay, respectively.

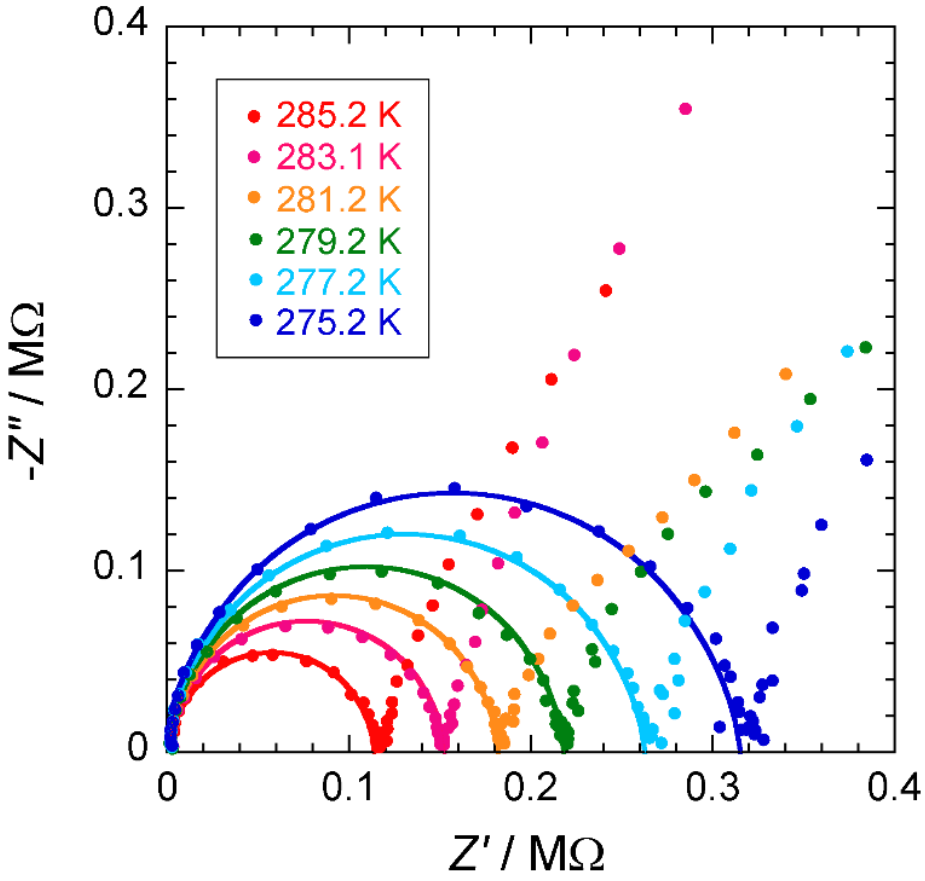


Figure 5. Nyquist plots of EIS measured at various temperatures in the single-crystalline TBAB semiclathrate hydrate (electrode area: 0.283 $cm^2$, distance between electrodes: 1.0 mm). The solid curves represent the fitting results by the first term of the equation (2).

**Ion conduction properties and identification of carrier ion**

The temperature dependences (Arrhenius plots) of the electrical conductivity and relaxation time obtained by EIS are shown in Figures 6 and 7, respectively. The values of electrical conductivity and relaxation time at 273, 278, and 283 K are listed in Table 1. The estimated activation energies in the electrical conductivity ($E_\sigma$) and electrical relaxation time ($E_\tau$) are also summarized in Table 2.

Figure 6 shows the electrical conductivity of TBAB semiclathrate hydrate and deuterate. TBAB semiclathrate hydrate had an electrical conductivity approximately 1.5 times higher than TBAB semiclathrate deuterate in the whole temperature range. These results reveal the isotope effect between TBAB semiclathrate hydrate and deuterate. The activation energy of electrical conductivity $E_\sigma$ in TBAB semiclathrate hydrate (62.2±0.3 kJ·mol$^{-1}$ (0.644±0.003 eV)) was slightly lower than that in TBAB semiclathrate deuterate one (63.6±0.2 kJ·mol$^{-1}$ (0.659±0.002 eV)). In ref. 22, the electrical conductivity at 250 K and activation energy $E_\sigma$ in a polycrystalline TBAB semiclathrate hydrate (TBAB·32$H_2O$), which was different from the composition in the present study (TBAB·26$H_2O$), were reported to be $1.8\times10^{-6}$ S·m$^{-1}$ and 43.4±0.3 kJ·mol$^{-1}$ (0.45±0.03 eV), respectively. It may be caused by either polycrystals used in ref. 22 or a single crystal used in the present study, not only the crystal structure.

The electrical conductivity in the semiclathrate hydrate would depend on the guest ionic species. In fact, tetramethylammonium hydroxide (TMAOH) and tetra-*n*-butylammonium hydroxide (TBAOH) semiclathrate hydrates exhibit high electrical conductivity according to the literature.[21-23,38] They possess a potential as solid electrolytes for batteries and hydrogen evolution materials to achieve the clean energy utilization.[23,38,26-28,43] Moreover, TMAOH semiclathrate hydrate has hydroxide anions ($OH^-$), which can withdraw protons ($H^+$) from

neighboring water molecules. This proton transfer would cause high proton conductivity. TBAOH semiclathrate hydrate, which has butyl groups longer than methyl groups in TMAOH, has also been reported to exhibit a high ionic conductivity.[26,28]

Figure 7 shows the electrical relaxation time of the single-crystalline TBAB semiclathrate hydrate and deuterate obtained by EIS. The electrical relaxation time in the TBAB semiclathrate deuterate was approximately 1.5 times as large as that in the TBAB semiclathrate hydrate, that is, the isotope effects were observed by deuterium substitution. The trend of the Arrhenius plots for the electrical relaxation time is similar to that of electrical conductivity (Figure 6). As shown in Table 2, the difference in the activation energies of electrical relaxation time ($E_\tau$) between TBAB semiclathrate hydrate (59.7±0.4 kJ·mol$^{-1}$, 0.618±0.004 eV) and TBAB semiclathrate deuterate (65.9±0.3 kJ·mol$^{-1}$, 0.683±0.003 eV) is a little.

The ratios of the isotope effect (approximately 1.5) obtained in the present study are close to the theoretical value originated from the mass ratio of proton to deuteron, which is estimated from classical kinetic model on the assumption of simple proton hopping conduction, as the following equation (6):[44-47]

$$\frac{\sigma_{\mathrm{H}}}{\sigma_{\mathrm{D}}} = \frac{\tau_{\mathrm{D}}}{\tau_{\mathrm{H}}} = \left(\frac{m_{\mathrm{H}}}{m_{\mathrm{D}}}\right)^{-1/2} = \sqrt{2} \qquad (6)$$

where $m_{\mathrm{H}}$ and $m_{\mathrm{D}}$ are the mass of proton and deuteron, respectively. The result indicates that the mass of hydrogen atom of the water molecules has a large effect on the mobility of carriers. In other words, hydrogen atoms of the water molecules contribute to the conduction mechanism in TBAB semiclathrate hydrate.

The temperature dependence of the relative permittivity at the top of frequencies in the Nyquist plots in single-crystalline TBAB semiclathrate hydrate was also estimated. Both the relative

permittivities were located around 130–140 in the temperature range of the present study. No significant differences in the relative permittivity between TBAB semiclathrate hydrate and TBAB semiclathrate deuterate were observed. It indicates that the increase in the mass of water molecules does not play a significant role in the polarization.

**Possible conduction mechanism in TBAB semiclathrate hydrates**

In ice Ih, it is well known that the proton conduction is distinctly classified into the Grotthuss and vehicle mechanisms.[48,49] The Grotthuss mechanism occurs mainly by the proton jumps through hydrogen-bonded networks between water molecules.[12] This is caused by the local molecular rearrangement, which allows the next jump. The rate-limiting is defined by rearrangement of hydrogen atom or proton in the Grotthuss mechanism. Vehicle mechanism is caused by the transfer of hydronium ions ($H_3O^+$), similar to the diffusion of water molecules. In this mechanism, molecular diffusion is rate-limiting step.

The isotope effect obtained in TBAB semiclathrate hydrate reveals that the proton is the carrier ion. However, it is difficult to discuss the detailed conduction mechanism only from the EIS results. There are three possible hypotheses of proton conduction mechanism, which provide kinetic isotope effect: 1) proton hopping via reorientation of water molecules (Grotthuss mechanism); 2) proton transfer by O-H stretching and bending motion (Grotthuss mechanism); 3) diffusion of hydronium ions (Vehicle mechanism). It is well known that the Grotthuss mechanism provides the isotope effect around 1.4 for electrical conductivity.[45,47] However, it is difficult only from the isotope effect to identify which conduction mechanism is dominant in the TBAB semiclathrate hydrate. As a possible technique to understand the conduction mechanism of proton in the TBAB semiclathrate hydrate, there might be solid-state $^1$H pulsed-

filed gradient NMR (PFG-NMR) measurement, which provides us the apparent diffusion coefficient of $^{1}H$ atom. Unfortunately, we cannot access the solid-state PFG-NMR that can measure such a fast diffusion. Therefore, we measured the solid-state $^{2}H$ NMR to help understand the dynamics of the water molecules in the TBAB semiclathrate hydrate and to figure out how similar the dynamics of the water molecules in the TBAB semiclathrate hydrate are to those in ice Ih.

**Water reorientation in TBAB semiclathrate deuterate investigated by NMR measurement**

The dynamics of the water molecules in ice Ih, especially reorientation motion, is considered as an important factor contributing to proton conduction, since the rate-limiting step has been considered to be the water reorientation motion in the icy materials.[12] To obtain the information of water reorientation motion, the spin-lattice ($T_1$) and spin-spin ($T_2$) relaxation times of $D_2O$ molecules in the TBAB semiclathrate deuterate were measured by solid-state $^{2}H$ NMR measurement.

The line shapes recorded by single-pulse sequence were displayed in Figure 8. The narrow peaks originated from the fast isotropic reorientational motion of $D_2O$ molecules were observed in the temperature range of 243–278 K, which are similar to the results reported in the literature.[50] As shown in inset figure in Figure 8, neither Pake-doublet powder pattern nor other broad peak was observed at these temperatures. It is consistent with the literature [50], where it was reported that the Pake-doublet powder pattern was observed only at temperatures below 225.2 K in the TBAB semiclathrate hydrate. In ice Ih, it is well known that the Pake-doublet powder pattern is observed even at temperatures slightly lower than the melting

point.[51] Thus, water dynamics in semiclathrate hydrate is considered to be more active and isotropic than that of ice system. The reason would be the existence of a large number of ions, which induce some defects in hydrogen-bonded water networks, in the TBAB semiclathrate hydrate.

$T_1$ and $T_2$ relaxation times obtained in the present study showed temperature dependence as shown in Figure 9. The $T_1$ recovery profile was an exponential type (see Figure S1), suggesting the almost homogenous state of deuterons in the semiclathrate sample. In fact, these results are in good agreement with the reported data [50]. Schildmann et al. reported not only $T_1$ and $T_2$ relaxation times but also the results by dielectric spectroscopy and stimulated-echo NMR experiment. Schildmann et al. [50] concluded comprehensively that the activation energy was 43±1 kJ·mol$^{-1}$, which differed from the results obtained in the present study (16.3±0.9 kJ·mol$^{-1}$). According to the ref. 50, however, there seems to be at least two different slopes in temperature dependences of $T_1$ relaxation time and reorientational correlation time. Comparing the results of $T_1$ relaxation times, the results obtained in the present study showed good agreement with the results [50] at temperatures above 220 K reported by Schildmann et al. They estimated the activation energy and pre-exponential coefficient in the whole temperature range without dividing into two temperature dependences at a border of 220 K. The disagreement of activation energies should be caused by the change of activation energies at a border of 220 K.

As a different analysis, the activation energy of half-width half-maximum (HWHM) of the narrow peak line width was examined (Figure 10).[39,40] As the results, the obtained activation energy was 20.3 kJ·mol$^{-1}$.

When we extrapolated the reorientation correlation time only above 220 K in ref. 50 by using the activation energy determined in the present study (16.3 kJ·mol$^{-1}$), the reorientation

correlation time of water molecules at 273 K was about 10 μs. This value is consistent with the relaxation time obtained from the EIS in the present study. From both NMR and EIS results, the relaxation times obtained by EIS may reflect the water reorientation time. Further investigation could elucidate the detail of the proton conduction mechanism.

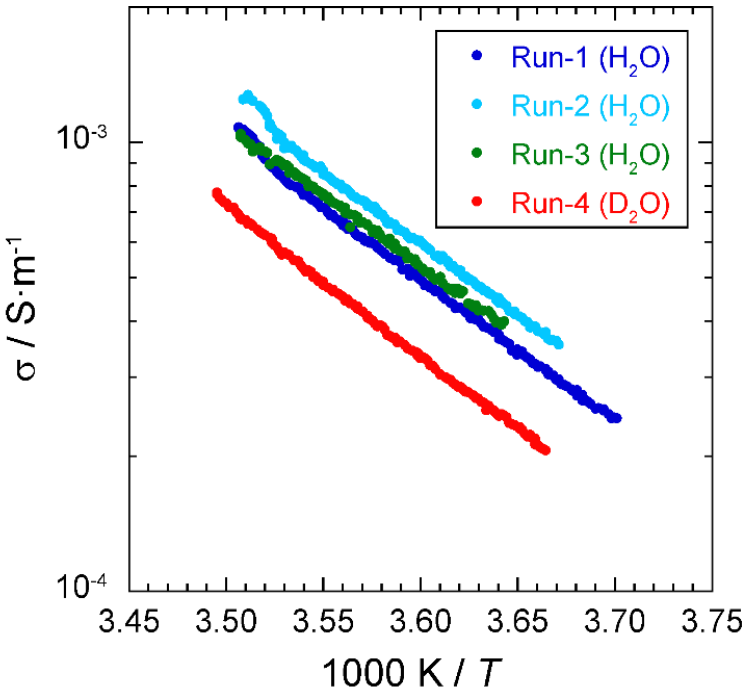


Figure 6. Arrhenius plots of the electrical conductivity in TBAB semiclathrate hydrate and TBAB semiclathrate deuterate.

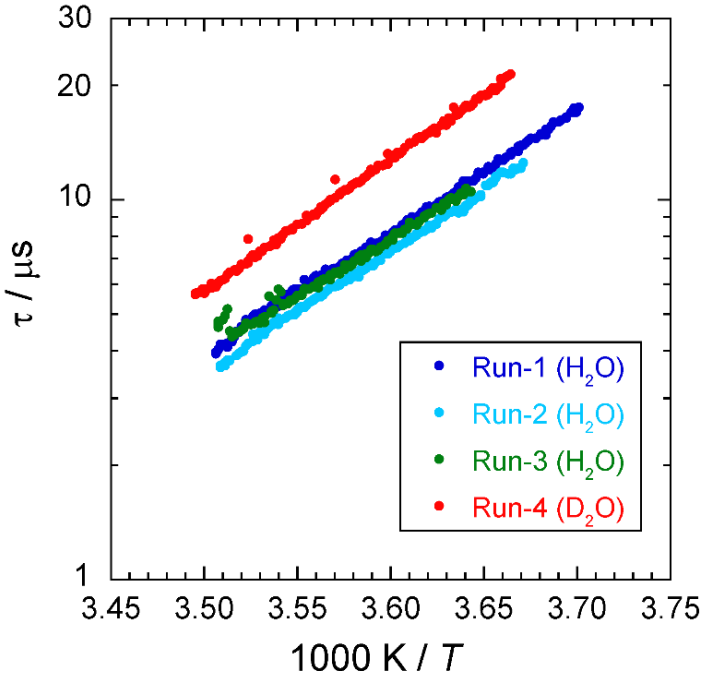


Figure 7. Arrhenius plots of the electrical relaxation time in TBAB semiclathrate hydrate and TBAB semiclathrate deuterate.

Table 1. Electrical conductivity (σ) and electrical relaxation time (τ) in TBAB semiclathrate hydrate and TBAB semiclathrate deuterate at 273, 278, and 283 K.

| | σ / mS·m$^{-1}$ | | | τ / μs | | |
|---|---|---|---|---|---|---|
| *T* / K | 273 | 278 | 283 | 273 | 278 | 283 |
| semiclathrate hydrate | 0.41 | 0.56 | 0.89 | 12 | 7.4 | 4.8 |
| semiclathrate deuterate | 0.21 | 0.35 | 0.56 | 21 | 12 | 7.3 |

Table 2. Activation energies of the electrical conductivity ($E_\sigma$) and electrical relaxation time ($E_\tau$) in TBAB semiclathrate hydrate and TBAB semiclathrate deuterate.

| | $E_\sigma$/ eV | $E_\sigma$/ kJ·mol$^{-1}$ | $E_\tau$/ eV | $E_\tau$ / kJ·mol$^{-1}$ |
|---|---|---|---|---|
| semiclathrate hydrate | 0.644 ±0.003 | 62.2 ±0.3 | 0.618 ±0.004 | 59.7 ±0.4 |
| semiclathrate deuterate | 0.659 ±0.002 | 63.6 ±0.2 | 0.683 ±0.003 | 65.9 ±0.3 |

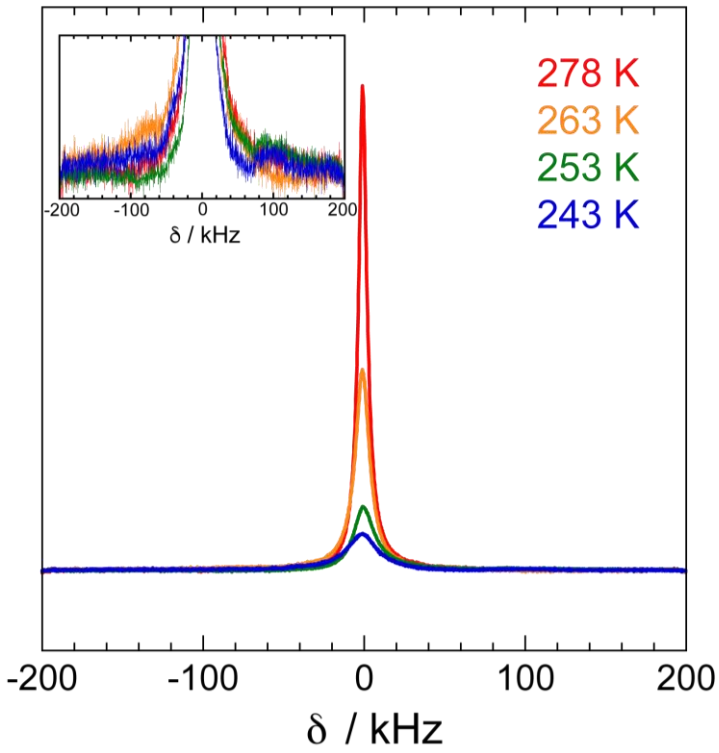


Figure 8. $^{2}$H NMR spectra of TBAB semiclathrate deuterate measured at 278 K, 263 K, 253 K, and 243 K. δ represents a chemical shift which was referred by pure heavy water. The narrow peaks reflect the fast water reorientation motion. The Pake-doublet was not observed even in the inset figure (enlarged view around baseline).

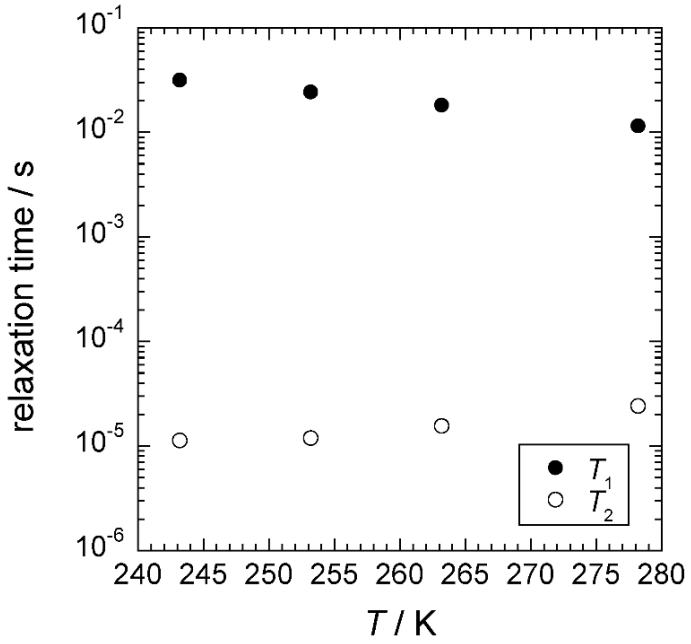


Figure 9. Temperature dependences of $^2$H spin-lattice relaxation time ($T_1$) and $^2$H spin-spin relaxation time ($T_2$).

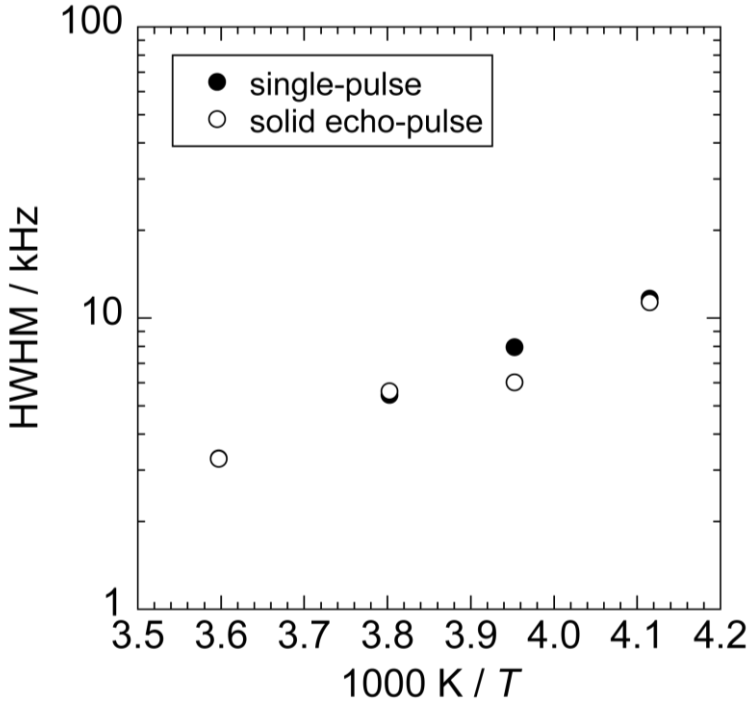


Figure 10. Temperature dependences of half-width half-maximum (HWHM) of narrow peaks measured by $^2$H single- and solid echo-pulse sequences.

## 4. CONCLUSIONS

In the present study, the electrochemical impedance spectra in the single-crystalline TBAB semiclathrate hydrate were measured. The electrochemical conductivity in TBAB semiclathrate hydrate was higher than that of ice Ih and showed Arrhenius-type temperature dependence. The isotope effects on the electrical conductivity and electrical relaxation time were clearly observed by EIS when the $D_2O$ was used instead of $H_2O$. The kinetic isotope effects reveal that the proton is the conduction carrier in the TBAB semiclathrate hydrate. For the proton conduction mechanism, Grotthuss and Vehicle mechanisms are known in icy materials. To discriminate the conduction mechanisms, we focused on the reorientation motion of water molecules. The reorientation time of water molecules in TBAB semiclathrate hydrate was determined by $T_1$ and $T_2$ relaxation by solid-state NMR measurements and is also in agreement with the relaxation time obtained by EIS. However, it is difficult to elucidate the conduction mechanism only from the results obtained in the present study.

## AUTHOR INFORMATION


### Corresponding Author

*TS: Tel and Fax: +81-6-6850-6293. E-mail: sugahara@cheng.es. osaka-u.ac.jp

*KT: Tel: +81 738 29 8413; Fax: +81-738-29-8439. E-mail: tsunashima@wakayama-nct.ac.jp

### ORCID

Takeshi Sugahara: 0000-0002-5236-5605

Katsuhiko Tsunashima: 0000-0002-4563-351X


### Notes

The authors declare no competing financial interest.

## ACKNOWLEDGMENT


This work was supported by JSPS KAKENHI Grant-in-Aid for JSPS Fellows (JP21J20788 for JS) and Grant-in-Aid for Scientific Research (JP17H03535 for AT, JP22K05050 for TS and JP19K05412 for KT). The solid-state NMR measurement were performed at the Analytical Instrument Facility, Graduate School of Science, Osaka University.


## REFERENCES


1. K. A. Kvenvolden, Gas hydrates—geological perspective and global change, *Rev. Geophys.*, 31 (1993) 173, https://doi.org/10.1029/93RG00268.
2. E. D. Sloan, C. A. Koh, in Clathrate Hydrates of Natural Gases, 3rd ed., CRC press, Boca Raton, FL, 2008.

3. J. S. Loveday, R. J. Nelmes, M. Guthrie, S. A. Belmonte, D. R. Allan, D. D. Klug, J. S. Tse, Y. P. Handa, Stable methane hydrate above 2 GPa and the source of Titan's stmospheric methane, *Nature*, 410 (2001) 661, https://doi.org/10.1038/35070513.

4. K. Kamata, F. Nimmo, Y. Sekine, K. Kuramoto, N. Noguchi, J. Kimura, A. Tani, Pluto's ocean is capped and insulated by gas hydrates, *Nature Geoscience*, 12 (2019) 407, https://doi.org/10.1038/s41561-019-0369-8.

5. M. Eigen, L. Maeyer, Self-Dissociation and Protonic Charge Transport in Water and Ice, *Proc. R. Soc. A* 247 (1958) 505, https://doi.org/10.1098/rspa.1958.0208.

6. M. Eigen, Proton Transfer, Acid-Base Catalysis, and Enzymatic Hydrosis. Part I: Elementary Processes, *Angew. Chem., Int. Ed. Engl.* 3 (1964) 1, https://doi.org/10.1002/anie.196400011.

7. C. Jaccard, Etude Theorique Et Experimentale Des Proprietes De La Glace, *Helv. Phys. Acta* 32 (1959) 89, https://doi.org/10.3929/ETHZ-A-000099624.

8. C. Jaccard, Thermodynamics of Irreversible Processes Applied to Ice, *Eur. Phys. J.* B 3 (1964) 99, https://doi.org/10.1007/BF02422356.

9. C. Jaccard, Mechanism of the Electrical Conductivity in Ice, *Ann. N. Y. Acad. Sci.* 125 (1965) 390. https://doi.org/10.1111/j.1749-6632.1965.tb45405.x.

10. L. Onsager, M. Dupuis, The Electrical Properties of Ice. In Electrolytes; Pesce, B., Ed.; Pergamon Press: Oxford (1962).

11. N. Bjerrum, Structure and Properties of Ice, *Science*, 115 (1952) 385, https://doi.org/10.1126/science.115.2989.385.

12. F. Bruni, G. Consolini, G. Careri, Temperature dependence of dielectric relaxation in $H_2O$ and $D_2O$ ice. A dissipative quantum tunneling approach, *J. Chem. Phys.*, 99 (1993) 538, https://doi.org/10.1063/1.465778.

13. Du Hyeong Lee, Heon Kang, Proton Transport and Related Chemical Processes of Ice, *J. Phys. Chem. B*, 125 (2021) 8270, https://doi.org/10.1021/acs.jpcb.1c04414.

14. L. A. Stern, S. Lu. R. Constable, W. L. Du Frane, J. J. Roberts, Electrical properties of carbon dioxide hydrate: Implications for monitoring $CO_2$ in the gas hydrate stability zone, *Geophysical Research Letters*, 48 (2021) e2021GL093475, https://doi.org/10.1029/2021GL093475

15. Z. Yin, J. Zheng, H. Kim, Y. Seo, P. Linga, Hydrates for cold energy storage and transport: A review, *Advances in Applied Energy*, 2 (2021), 100022, https://doi.org/10.1016/j.adapen.2021.100022.

16. Y. A. Dyadin, K. A. Udachin, Clathrate polyhydrates of peralkylonium salts and their analogs, *J. Struct. Chem.*, 28 (1987) 394, https://doi.org/10.1007/BF00753818.

17. D. L. Fowler, W. V. Loebenstein, D. B. Pall, C. A. Kraus, Some Unusual Hydrates of Quaternary Ammonium Salts, *J. Am. Chem. Soc.*, 62 (1940) 1140, https://doi.org/10.1021/ja01862a039.

18. W. Shimada, M. Shiro, H. Kondo, S. Takeya, H. Oyama, T. Ebinuma, H. Narita, Tetra-*n*-butyl-ammonium bromide-water (1/38), *Acta Crystallogr., Sect. C: Cryst. Struct. Commun.*, 61 (2005) o65, https://doi.org/10.1107/S0108270104032743

19. S. Muromachi, S. Takeya, Y. Yamamoto, R. Ohmura, Characterization of tetra-*n*-butylphosphonium bromide semiclathrate hydrate by crystal structure analysis, *CrystEngComm*, 16 (2014) 2056. https://doi.org/10.1039/C3CE41942H.

20. T. V. Rodionova, I. S. Terekhova, A. Y. Manakov, Ionic Clathrate Hydrates of Tetraalkylammonium/phosphonium Salts: Structures, Properties, Some Applications, and Perspectives, Energy Fuels 36 (2022) 18, 10458, https://doi.org/10.1021/acs.energyfuels.2c01221.

21. Z. Borkowska, A. Tymosiak, M. Opallo, Conductivity of stoichiometric $(CH_3)_4NOH$ clathrate hydrates, *J. Electroanal. Chem.,* 406 (1996) 109, https://doi.org/10.1016/0022-0728(95)04425-6.

22. M. Opallo, A. Tymosiak-Zielinska, Z. Borkowska, Tetra-alkylammonium cation clathrate hydrates as novel proton conductors, *Solid State Ionics*, 97 (1997) 247, https://doi.org/10.1016/S0167-2738(97)00080-5.

23. A. Prokopowicz, M. Opallo, Electrical and electrochemical processes in solid tetrabutylammonium hydroxide hydrate, *Solid State Ionics*, 145 (2001) 407, https://doi.org/10.1016/S0167-2738(01)00937-7.

24. M. Opallo, Z. Borkowska, P. Zoltowski, A. Tymosiak, Electrical Properties of Ionic Conductor below and above Melting Point. Tetraalkylammonium Cation Hydrate, *Solid State Phenomena*, 39 (1994) 321, https://doi.org/10.4028/www.scientific.net/SSP.39-40.321.

25. M. Opallo, A. Tymosiak, Z. Borkowska, Conductivity of tetramethylammonium fluoride tetrahydrate, *J. Electroanal. Chem.*, 387 (1995) 47, https://doi.org/10.1016/0022-0728(95)03859-F.

26. A. Prokopowicz, M. Opallo, Electrochemical hydrogen evolution from solid tetraalkylammonium hydroxide hydrates, *Solid State Ionics*, 157 (2003) 209, https://doi.org/10.1016/S0167-2738(03)00259-5.

27. M. Opallo, A. Prokopowicz, Electrochemical hydrogen evolution in hydroxide hydrate down to 110 K, *Electrochem. Commum.*, 2 (2000) 23, https://doi.org/10.1016/S1388-2481(99)00134-4.

28. A. Prokopowicz, M. Opallo, Electrochemical hydrogen evolution from solid tetraalkylammonium hydroxide hydrates, *Solid State Ionics*, 162 (2003) 231, https://doi.org/10.1016/S0167-2738(03)00259-5.

29. M. Gerstl, E. Navickas, G. Friedbacher, F. Kubel, M. Ahrens, J. Fleig, The separation of grain and grain boundary impedance in thin yttria stabilized zirconia (YSZ) layers, *Solid State Ionics*, 185 (2011) 32, https://doi.org/10.1016/j.ssi.2011.01.008.

30. T. Sugahara, H. Machida, Dissociation and Nucleation of Tetra-*n*-butyl Ammonium Bromide Semi-Clathrate Hydrates at High Pressures, *J. Chem. Eng. Data*, 62 (2017) 2721, https://doi.org/10.1021/acs.jced.7b00115.

31. T. V. Rodionova, V. Yu. Komarov, G. V. Villevald, T. D. Karpova, N. V. Kuratieva, A. Yu. Manakov, Calorimetric and Structural Studies of Tetrabutylammonium Bromide Ionic Clathrate Hydrates, *J. Phys. Chem. B*, 117 (2013) 10677, https://doi.org/10.1021/jp406082z.

32. X. Zhou, D. Liang, Enhanced performance on $CO_2$ adsorption and release induced by structural transition that occurred in TBAB·26$H_2O$ hydrates, *Chem. Eng. J.*, 378 (2019) 122128, https://doi.org/10.1016/j.cej.2019.122128.

33. H. Oyama, W. Shimada, T. Ebinuma, Y. Kamata, S. Takeya, T. Uchida, J. Nagao, H. Narita, Phase diagram, latent heat, and specific heat of TBAB semiclathrate hydrate crystals, *Fluid Phase Equilib.*, 234 (2005) 131, https://doi.org/10.1016/j.fluid.2005.06.005.

34. J. Deschamps, D. D. Dalmazzone, Hydrogen Storage in Semiclathrate Hydrates of Tetrabutyl Ammonium Chloride and Tetrabutyl Phosphonium Bromide, *J. Therm. Anal. Calorim.,* 98 (2009) 113, https://doi.org/10.1021/je100146b.

35. Gaponenko, L. A.; Solodovnikov, S. F.; Dyadin, Yu. A.; Aladko, L. S.; Polyanskaya, T. M. Crystallographic Study of Tetra-*n*-butylammonium Bromide Polyhydrates. *J. Struct. Chem.* 25 (1984) 157.

36. Ph. Colomban, A. Novak, Proton transfer and superionic conductivity in solids and gels, *J. Mol. Struct.,* 177 (1988) 277, https://doi.org/10.1016/0022-2860(88)80094-2.

37. Ph. Colomban, J. C. Badot, M. Pham-Thi, A. Novak, Defects, phase transitions and dynamical disorder in superionic protonic conductors $H_3OUO_2PO_4 \cdot 3H_2O$ and $CsHSO_4$, *Phase Transitions*, 14 (1989) 1, https://doi.org/10.1080/01411598908208081.

38. N. Kuriyama, T. Sakai, H. Miyamura, A. Kato, H. Ishikawa, High conductivity and phase transitions of tetramethylammonium hydroxide pentahydrate, $(CH_3)_4NOH \cdot 5H_2O$, *Solid State Ionics*, 40/41 (1990) 906, https://doi.org/10.1016/0167-2738(90)90150-P.

39. A. Abragam, in Principles of nuclear magnetism, Oxford University Press, Oxford, 1961.

40. H. Omichi, T. Ueda, T. Eguchi, Molecular motion of alcohols adsorbed in ACF hydrophobic nanoslits as studied by solid-state NMR, *Adsorption*, 21 (2015) 273, https://doi.org/10.1007/s10450-015-9669-5.

41. Y. Tsuchida, M. Matsumiya, K. Tsunashima, Preparation of polymer electrolytes using ionic liquids and evaluation of physicochemical properties, *J. Mol. Liq.*, 15 (2019) 204, https://doi.org/10.1016/j.molliq.2018.10.101.

42. Z. Wu, Z. Xie, J. Wang, T. Yu, Z. Wang, X. Hao, A. Abudula, G. Guan, Lithium-Salt-Containing Ionic Liquid-Incorporated Li–Al-Layered Double Hydroxide-Based Solid Electrolyte with High-Performance and Safety in Solid-State Lithium Batteries, *ACS Sustainable Chem. Eng.*, 8 (2020) 12378, https://doi.org/10.1021/acssuschemeng.0c02362.

43. N. Kuriyama, T. Sakai, H. Miyamura, H. Ishikawa, Solid-state metal hydride batteries using tetramethylammonium hydroxide pentahydrate, *Solid State Ionics*, 53 (1992) 688, https://doi.org/10.1016/0167-2738(92)90448-X.

44. D. Kek, N. Bonanos, Electrochemical H–D isotope effect at metal–perovskite proton conductor interfaces, *Solid State Ionics*, 125 (1999) 345, https://doi.org/10.1016/S0167-2738(99)00195-2.

45. N. Agmon, The Grotthuss mechanism, *Chem. Phys. Lett.* 244 (1995) 456, https://doi.org/10.1016/0009-2614(95)00905-J.

46. A.S. Nowick , A.V. Vaysleyb, Isotope effect and proton hopping in high-temperature protonic conductors, *Solid State Ionics* 97 (1997) 17, https://doi.org/10.1016/S0167-2738(97)00081-7.

47. S. Østby Stub, E. Vøllestad, T. Norby*, Mechanisms of Protonic Surface Transport in Porous Oxides: Example of YSZ, *J. Phys. Chem. C*, 121 (2017) 12817, https://doi.org/10.1021/acs.jpcc.7b03005.G.

48. A. Ludueña, T. D. Kühne, D. Sebastiani, Mixed Grotthuss and Vehicle Transport Mechanism in Proton Conducting Polymers from Ab initio Molecular Dynamics Simulations, *Chem. Mater.*, 23 (2011) 1424, https://doi.org/10.1021/cm102674u.

49. Q. Li, Q. Yin, Y. S. Zheng, Z. J. Sui, X. G. Zhou, D. Chen, Y. A. Zhu, Q. Li, Q. Yin, Y. S. Zheng, Z. J. Sui, X. G. Zhou, D. Chen, Y. A. Zhu, Insights into Hydrogen Transport Behavior on Perovskite Surfaces: Transition from the Grotthuss Mechanism to the Vehicle Mechanism, *Langmuir*, 35 (2019) 9962, https://doi.org/10.1021/acs.langmuir.8b04138.S.

50. Schildmann, A. Nowaczyk, B. Geil, C. Gainaru, R. Böhmer, Water dynamics on the hydrate lattice of a tetrabutyl ammonium bromide semiclathrate, *J. Chem. Phys*., 130 (2009) 104505, https://doi.org/10.1063/1.3081897.

51. C. Totland, S. Steinkopf, A. M. Blokhus, W. Nerdal, Water Structure and Dynamics at a Silica Surface: Pake Doublets in $^{1}$H NMR Spectra, *Langmuir*, 27 (2011) 4690, https://doi.org/10.1021/la1048997.